

Accuracy of Homology based Coverage Hole Detection for Wireless Sensor Networks on Sphere

Feng Yan, *Member, IEEE*, Philippe Martins, *Senior Member, IEEE*, and Laurent Decreasefond

Abstract—Homology theory has attracted great attention because it can provide novel and powerful solutions to address coverage problems in wireless sensor networks. They usually use an easily computable algebraic object, Rips complex, to detect coverage holes. But Rips complex may miss some coverage holes in some cases. In this paper, we investigate homology-based coverage hole detection for wireless sensor networks on sphere. The case when Rips complex may miss coverage holes is first identified. Then we choose the proportion of the area of coverage holes missed by Rips complex as a metric to evaluate the accuracy of homology-based coverage hole detection approaches. Closed-form expressions for lower and upper bounds of the accuracy are derived. Asymptotic lower and upper bounds are also investigated when the radius of sphere tends to infinity. Simulation results are well consistent with the analytical lower and upper bounds, with maximum differences of 0.5% and 3% respectively. Furthermore, it is shown that the radius of sphere has little impact on the accuracy if it is much larger than communication and sensing radii of each sensor.

Index Terms—Wireless sensor networks, coverage hole, homology.

I. INTRODUCTION

WIRELESS sensor networks (WSNs) have attracted considerable research attention due to their large number of potential applications such as battlefield surveillance, environmental monitoring and intrusion detection. Many of these applications require a reliable detection of specified events. Such requirement can be guaranteed only if the target field monitored by a WSN contains no coverage holes, that is to say regions of the domain not monitored by any sensor. But coverage holes can be formed for many reasons, such as random deployment, energy depletion or destruction of sensors. Consequently, it is essential to detect and localize coverage holes in order to ensure the full operability of a WSN.

Most existing works on coverage hole issues mainly focus on two-dimensional (2D) plane or three-dimensional (3D) full space. There is few work on 3D surfaces. But in some real applications, such as volcano monitoring [1] and forest monitoring [2], the target fields are complex surfaces. So it is also important to consider the coverage hole detection problem of WSNs on surfaces. On the other hand, from theoretical point of view, the coverage on 3D surfaces is quite a different

problem from its counterpart in 2D plane or 3D full space. As sphere is the simplest case of 3D surfaces, we choose it as the first step for the analysis in this paper, like the authors did in [3] for throughput capacity analysis.

There are already extensive works on the coverage hole detection problem for WSNs in 2D plane and 3D space. Some of these works used either precise information about sensor locations [4]–[8] or accurate relative distances between neighbouring sensors [9], [10] to detect coverage holes. The requirement of precise location or distance information substantially limits their applicability since acquiring such information is either expensive or impractical in many settings. Thus connectivity-based approaches are of great interest for us. In this category, homology-based schemes have received special attention because of its powerfulness for coverage hole problems in WSNs.

Homology theory was first adopted by Ghrist and his collaborators in [11]–[13] to address the coverage problems in WSNs. They introduced a combinatorial object, Čech complex, which uses sensing ranges of nodes to fully characterize coverage properties of a WSN (existence and locations of holes). Unfortunately, the construction of this object is of very high complexity [14] even if the precise location information about sensors is provided. Thus, they introduced another more easily computable complex, Vietoris-Rips complex (we will abbreviate the term to Rips complex in this paper). This complex is constructed with the sole knowledge of the connectivity graph of the network and gives an approximate coverage by simple algebraic calculations. Considering the ease of Rips complex construction, some homology-based algorithms were proposed in [15]–[17] to use Rips complex to detect coverage holes. But all these homology-based approaches do not consider the cases that Rips complex may miss some special coverage holes. If the proportion of the area of coverage holes missed by Rips complex is low enough, then it is acceptable to use these methods for coverage hole detection. If the proportion is too high to be unacceptable, then it may not be proper to use these methods. Therefore, in order to evaluate the accuracy of homology-based coverage hole detection approaches, it is of paramount importance to analyse the coverage holes missed by Rips complex.

The main contributions of our paper are as follows. First, the relationship between Čech complex and Rips complex in terms of coverage hole on sphere is analysed. Furthermore, the case that Rips complex may miss coverage holes is identified and it is found that a hole in a Čech complex missed by a Rips complex must be bounded by a spherical triangle. Based on that, a formal definition of spherical triangular hole is given.

F. Yan was with the Network and Computer Science Department, TELECOM ParisTech, Paris, France. He is currently with the Networks, Security and Multimedia Department, TELECOM Bretagne, Rennes, France. (e-mail: feng.yan@telecom-bretagne.eu)

P. Martins and L. Decreasefond are with the Network and Computer Science Department, TELECOM ParisTech, Paris, France. (e-mail: martins@telecom-paristech.fr, decrease@telecom-paristech.fr.) A part of this paper has been published in IEEE ICC 2012.

Second, the proportion of the area of spherical triangular holes is chosen as a metric to evaluate the accuracy of homology-based coverage hole detection. Such proportion is analysed under a homogeneous setting and it is related to the communication and sensing radii of each sensor. Closed-form expressions for lower and upper bounds of the proportion are derived. Asymptotic lower and upper bounds are also investigated when the radius of sphere tends to infinity.

Third, extensive simulations are performed to evaluate impacts of communication and sensing radii, radius of sphere on proportion of the area of spherical triangular holes. It is shown that simulation results are well consistent with the analytical lower bound, with a maximum difference of 0.5%, and consistent with the analytical upper bound, with a maximum difference of 3%. Furthermore, simulation results show that the radius of sphere has little impact on the proportion when it is much larger than communication and sensing radii.

The rest of the paper is organised as follows. Section II presents the related work. In Section III, the network model and the formal definition of spherical triangular hole are given. Closed-form lower and upper bounds for proportion of the area of spherical triangular holes are derived in Section IV. Section V compares simulation results and analytical bounds. Finally, Section VI concludes the paper.

II. RELATED WORK

Since this paper aims to evaluate the ratio of the area of coverage holes missed by homology-based approaches, we present the related work in terms of two aspects: coverage hole detection approaches and analytical coverage ratio evaluation.

A. Coverage hole detection approaches

Many approaches have been proposed for coverage hole detection in WSNs. They can be generally classified into three categories: location-based, range-based and connectivity-based.

Location-based approaches are usually based on computational geometry with tools such as Voronoi diagram and Delaunay triangulations, to discover coverage holes [4]–[6]. Range-based approaches attempt to discover coverage holes by using only relative distances between neighbouring sensors [9], [10]. These two types of approaches need either precise location information or accurate distance information, which restricts their applications since such information is not easy to obtain in many settings.

In connectivity-based approaches, homology-based schemes attract particular attention due to its powerfulness for coverage hole detection. De Silva *et al.* first proposed a centralized algorithm that detects coverage hole via homology in [12]. They constructed the Rips complex corresponding to the communication graph of the network and determined the coverage by verifying whether the first homology group of the Rips complex is trivial. Then the above ideas were first implemented in a distributed way in [15]. It is shown that combinatorial Laplacians are the right tools for distributed computation of homology groups and can be used for decentralized coverage verification. In [16], a gossip-like decentralized algorithm for

computation of homology groups was proposed. In [17], a decentralized scheme based on Laplacian flows was proposed to compute a generator of the first homology group. All these homology-based algorithms may be also used to detect coverage holes for WSNs on surfaces, but they do not consider the cases that Rips complex may miss some special coverage holes. One of our objectives in this paper is to identify such cases.

B. Analytical coverage ratio evaluation

Extensive research has been done to analyse coverage ratio of a WSN in 2D plane or on 3D surfaces. In [18], the authors studied the coverage properties of large-scale sensor networks and obtained the fraction of the area covered by sensors. The sensors are assumed to have the same sensing range and are distributed according to a homogeneous Poisson point process (PPP) in plane. In [19], the authors studied how the probability of k -coverage changes with the sensing radius or the number of sensors, given that sensors are deployed as either a PPP or a uniform point process. In addition, the distance distribution between two points in random networks was derived in [20]. Their results can be used to derive the fraction of areas covered by at least k -sensors. All the above studies only considered homogeneous cases. In [21], the coverage problem in planar heterogeneous sensor networks are investigated and analytical expressions of coverage are derived. Their formulation is more general in the sense that sensor can be deployed according to an arbitrary stochastic distribution, or can have different sensing capabilities or can have arbitrary sensing shapes. Based on their results, the authors in [22] derived the expected coverage ratio of sensors under stochastic deployment on 3D surface. Similarly, the expected coverage ratio under stochastic deployment on 3D rolling terrains was derived in [23]. In [24], a point in a plane is defined to be tri-covered if it lies inside a triangle formed by three nodes, and the probability of tri-coverage was analysed.

All the above research considered only coverage ratio problems, without considering coverage hole detection issues. Their analysis is thus not specific to any coverage hole detection approaches. We provided some initial results about the proportion of the area of triangular holes for WSNs in 2D plane in [25]. In this paper, we aim to analyse the proportion of the area of coverage holes missed by homology-based coverage hole detection approaches for WSNs on sphere and compare it with the case in 2D plane.

III. MODELS AND DEFINITIONS

Consider a collection of stationary sensors (also called nodes) on a sphere \mathbb{S}^2 with radius R . The sensors are deployed according to a homogeneous PPP with intensity λ . For any two points p_1 and p_2 on \mathbb{S}^2 , the distance between them $d(p_1, p_2)$ is defined to be the great circle distance, which is the shortest distance between them measured along a path on the surface of the sphere. As usual, isotropic radio propagation is assumed. All sensors have the same sensing radius R_s and communication radius R_c on \mathbb{S}^2 . It means for any sensor located at v on \mathbb{S}^2 , any point p on \mathbb{S}^2 with $d(v, p) \leq R_s$ is

inside the sensing range of the sensor; and for any two sensors located at v_i, v_j on \mathbb{S}^2 , they can communicate with each other if $d(v_i, v_j) \leq R_c$. In addition, we assume $R_s \ll R, R_c \ll R$.

Before defining the two combinatorial objects, known as Čech complex and Rips complex, it is necessary to give a brief introduction to some tools used in the paper. For further readings, see [26]–[28]. Given a set of points V , a k -simplex is an unordered set $[v_0, v_1, \dots, v_k] \subseteq V$ where $v_i \neq v_j$ for all $i \neq j$, k is the dimension of this simplex. The faces of this k -simplex consist of all $(k-1)$ -simplex of the form $[v_0, \dots, v_{i-1}, v_{i+1}, \dots, v_k]$ for $0 \leq i \leq k$. For example, on a sphere \mathbb{S}^2 , a 0-simplex $[v_0]$ is a vertex, a 1-simplex $[v_0, v_1]$ is the shorter arc of the great circle passing through v_0 and v_1 , a 2-simplex $[v_0, v_1, v_2]$ is a spherical triangle $v_0v_1v_2$ with its interior included, see Figure 1. An abstract simplicial complex is a collection of simplices which is closed with respect to inclusion of faces. A k -dimensional abstract simplicial complex \mathcal{K} is an abstract simplicial complex where the largest dimension of any simplex in \mathcal{K} is k .

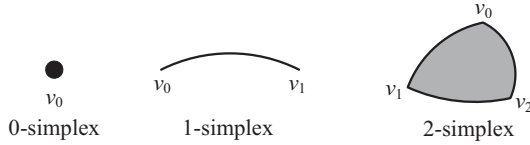


Fig. 1. 0-, 1- and 2-simplex

Let \mathcal{V} denote the set of sensor locations in a WSN on \mathbb{S}^2 with radius R and $\mathcal{S} = \{s_v, v \in \mathcal{V}\}$ denote the collection of sensing ranges of these sensors: for a location v , $s_v = \{x \in \mathbb{S}^2 : d(x, v) \leq R_s\}$. Then Čech complex and Rips complex can be defined as follows [11], [12].

Definition 1 (Čech complex). *Given a finite collection of sensing ranges $\{s_v, v \in \mathcal{V}\}$, the Čech complex of the collection, $\check{C}(\mathcal{V})$, is the abstract simplicial complex whose k -simplices correspond to non-empty intersections of $k + 1$ distinct elements of $\{s_v, v \in \mathcal{V}\}$.*

Definition 2 (Rips complex). *Given a finite set of points \mathcal{V} on \mathbb{S}^2 and a fixed radius ϵ , the Rips complex of \mathcal{V} , $\mathcal{R}_\epsilon(\mathcal{V})$, is the abstract simplicial complex whose k -simplices correspond to unordered $(k + 1)$ -tuples of points in \mathcal{V} which are pairwise within distance ϵ of each other.*

According to the definitions, the Čech complex and Rips complex of the WSN, respectively denoted by $\check{C}_{R_s}(\mathcal{V})$ and $\mathcal{R}_{R_c}(\mathcal{V})$, can be constructed as follows: a k -simplex $[v_0, v_1, \dots, v_k]$ belongs to $\check{C}_{R_s}(\mathcal{V})$ whenever $\bigcap_{l=0}^k s_{v_l} \neq \emptyset$ and a k -simplex $[v_0, v_1, \dots, v_k]$ belongs to $\mathcal{R}_{R_c}(\mathcal{V})$ whenever $d(v_l, v_m) \leq R_c$ for all $0 \leq l < m \leq k$. In addition, since we consider only coverage holes on the sphere \mathbb{S}^2 , it is sufficient to construct 2-dimensional Čech complex and 2-dimensional Rips complex of the WSN, denoted as $\check{C}_{R_s}^{(2)}(\mathcal{V})$ and $\mathcal{R}_{R_c}^{(2)}(\mathcal{V})$ respectively.

Figure 2 shows a WSN, its Čech complex and two Rips complexes for two different values of R_c . Depending on the relation of R_c and R_s , the Rips complex and the Čech complex may be close or rather different. In this example, for $R_c =$

$2R_s$, the Rips complex sees the hole surrounded by 2, 3, 5, 6 as in the Čech complex whereas it is missed in the Rips complex for $R_c = 2.5R_s$. At the same time, the true coverage hole surrounded by 1, 2, 6 is missed in both Rips complexes.

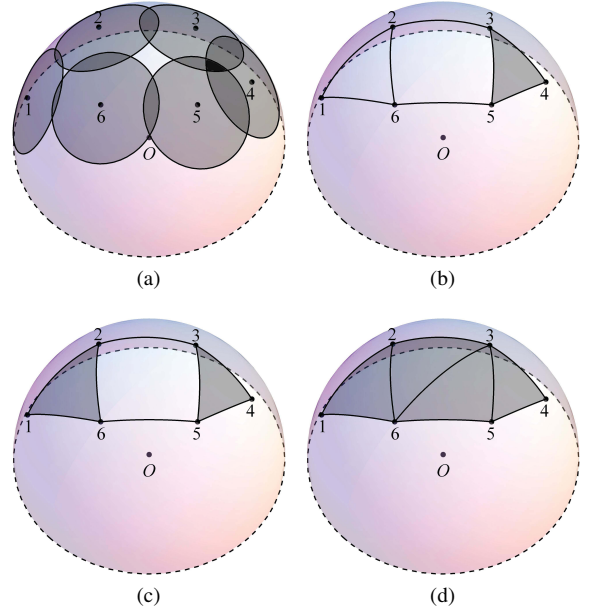


Fig. 2. (a) a WSN, (b) Čech complex, (c) Rips Complex under $R_c = 2R_s$, (d) Rips Complex under $R_c = 2.5R_s$

In fact, as proved in [29], any coverage hole can be found in Čech complex. Unfortunately, the construction of Čech complex is of very high complexity even if the precise location information of nodes is provided. So a more easily computable tool, Rips complex, is used. But Rips complex can not always capture all coverage holes. To be more specific, there exist following relations between $\check{C}_{R_s}^{(2)}(\mathcal{V})$ and $\mathcal{R}_{R_c}^{(2)}(\mathcal{V})$.

Lemma 1. *Let \mathcal{V} denote the set of node locations in a WSN on \mathbb{S}^2 with radius R , all nodes have the same sensing radius R_s and communication radius R_c , $R_s \ll R, R_c \ll R$, then*

$$\mathcal{R}_{R_c}^{(2)}(\mathcal{V}) \subset \check{C}_{R_s}^{(2)}(\mathcal{V}) \subset \mathcal{R}_{2R_s}^{(2)}(\mathcal{V}), \quad (1)$$

whenever $R_c \leq R \arccos([3 \cos^2(R_s/R) - 1]/2)$

Proof: See the Appendix A. ■

According to (1), some relationships between Čech complex and Rips complex in terms of coverage hole can be derived as illustrated in the following corollaries.

Corollary 1. *When $R_c \leq R \arccos([3 \cos^2(R_s/R) - 1]/2)$, if there is no hole in $\mathcal{R}_{R_c}^{(2)}(\mathcal{V})$, there must be no hole in $\check{C}_{R_s}^{(2)}(\mathcal{V})$.*

Corollary 2. *When $R_c \geq 2R_s$, if there is a hole in $\mathcal{R}_{R_c}^{(2)}(\mathcal{V})$, there must be a hole in $\check{C}_{R_s}^{(2)}(\mathcal{V})$.*

Corollary 3. *When $R \arccos([3 \cos^2(R_s/R) - 1]/2) < R_c < 2R_s$, there is no guarantee relation between $\check{C}_{R_s}^{(2)}(\mathcal{V})$ and $\mathcal{R}_{R_c}^{(2)}(\mathcal{V})$.*

From Corollary 1, a sufficient condition for coverage verification can be derived. From Corollary 2, we can find a

necessary condition for the existence of a hole in $\check{C}_{R_s}^{(2)}(\mathcal{V})$. Corollary 3 indicates that when there is no hole in $\mathcal{R}_{R_c}^{(2)}(\mathcal{V})$, it is possible that there is a hole in $\check{C}_{R_s}^{(2)}(\mathcal{V})$. When there is a hole in $\mathcal{R}_{R_c}^{(2)}(\mathcal{V})$, it is also possible that $\check{C}_{R_s}^{(2)}(\mathcal{V})$ contains no hole. From these corollaries, it can be seen that when $R_c > R \arccos([3 \cos^2(R_s/R) - 1]/2)$, $\mathcal{R}_{R_c}^{(2)}(\mathcal{V})$ may miss a hole in $\check{C}_{R_s}^{(2)}(\mathcal{V})$. Furthermore, a hole in a $\check{C}_{R_s}^{(2)}(\mathcal{V})$ not seen in a $\mathcal{R}_{R_c}^{(2)}(\mathcal{V})$ must be bounded by a spherical triangle. Based on this observation, a formal definition of spherical triangular hole is given as follows.

Definition 3 (Spherical triangular hole). *For a pair of complexes $\check{C}_{R_s}^{(2)}(\mathcal{V})$ and $\mathcal{R}_{R_c}^{(2)}(\mathcal{V})$ of a WSN, a spherical triangular hole is an uncovered region bounded by a spherical triangle formed by three nodes v_0, v_1, v_2 , where v_0, v_1, v_2 can form a 2-simplex which appears in $\mathcal{R}_{R_c}^{(2)}(\mathcal{V})$ but not in $\check{C}_{R_s}^{(2)}(\mathcal{V})$.*

According to Definition 3, it can be seen from Figure 2 that when $R_c = 2R_s$, there is one spherical triangular hole bounded by the spherical triangle formed by nodes 1, 2 and 6. And when $R_c = 2.5R_s$, there are two additional spherical triangular holes, bounded by spherical triangles formed by nodes 2, 3, 6 and 3, 5, 6 respectively.

A summary of the main notations is given in Table I.

TABLE I
MAIN NOTATIONS

| symbols | meaning |
|--|---|
| R_s | sensing radius of each sensor |
| R_c | communication radius of each sensor |
| R | the radius of sphere where sensors are deployed |
| \mathcal{V} | the set of sensor locations |
| s_v | the sensing range of the sensor located at v |
| \mathcal{S} | collection of sensing ranges of sensors in \mathcal{V} |
| $\check{C}_{R_s}^{(2)}(\mathcal{V})$ | 2-dimensional Čech complex of the WSN denoted by \mathcal{V} |
| $\mathcal{R}_{R_c}^{(2)}(\mathcal{V})$ | 2-dimensional Rips complex of the WSN denoted by \mathcal{V} |
| λ | the intensity of Poisson point process |
| $p(\lambda)$ | the probability of any point on sphere being inside a spherical triangular hole |
| $p_l(\lambda)$ | lower bound of $p(\lambda)$ |
| $p_u(\lambda)$ | upper bound of $p(\lambda)$ |
| $p'_l(\lambda)$ | asymptotic lower bound of $p(\lambda)$ when $R \rightarrow \infty$ |
| $p'_u(\lambda)$ | asymptotic upper bound of $p(\lambda)$ when $R \rightarrow \infty$ |

IV. BOUNDS ON PROPORTION OF SPHERICAL TRIANGULAR HOLES

In this section, the conditions under which any point on \mathbb{S}^2 with radius R is inside a spherical triangular hole are first given. The proportion of the area of spherical triangular holes is chosen as a metric for accuracy evaluation. Closed-form expressions for lower and upper bounds of the proportion are derived. Finally, the asymptotic lower and upper bounds are investigated when the radius of sphere tends to infinity.

A. Preliminary

Lemma 2. *For any point on \mathbb{S}^2 , it is inside a spherical triangular hole if and only if the following two conditions are satisfied:*

- 1) *the great circle distance between the point and its closest node is larger than R_s .*
- 2) *the point is inside a spherical triangle: the convex hull of three nodes with pairwise great circle distance less than or equal to R_c .*

Lemma 3. *If there exists a point O which is inside a spherical triangular hole, then $R_s < R \arccos \sqrt{[1 + 2 \cos(R_c/R)]/3}$.*

Proof: According to Definition 3, if there is a point O inside a spherical triangular hole, then there exists a 2-simplex $\sigma \in \mathcal{R}_{R_c}^{(2)}(\mathcal{V})$ while $\sigma \notin \check{C}_{R_s}^{(2)}(\mathcal{V})$, so $\mathcal{R}_{R_c}^{(2)}(\mathcal{V}) \not\subset \check{C}_{R_s}^{(2)}(\mathcal{V})$. According to (1), we have $R_c > R \arccos([3 \cos^2(R_s/R) - 1]/2) \Rightarrow R_s < R \arccos \sqrt{[1 + 2 \cos(R_c/R)]/3}$. ■

Lemma 4. *Let O be a point inside a spherical triangular hole and l denote the great circle distance between O and its closest neighbour, then $R_s < l \leq R \arccos \sqrt{[1 + 2 \cos(R_c/R)]/3}$.*

The proof is similar as that of Lemma 1.

Since nodes are assumed to be distributed on \mathbb{S}^2 according to a homogeneous Poisson point process with intensity λ , any point has the same probability to be inside a spherical triangular hole. This probability in a homogeneous setting is also equal to the proportion of the area of spherical triangular holes.

We use spherical coordinates (R, θ, φ) to denote points on \mathbb{S}^2 with radius R , where θ is polar angle and φ is azimuth angle. Without loss of generality, we consider the probability of the point N with spherical coordinates $(R, 0, 0)$ being inside a spherical triangular hole. Since the communication radius of each sensor is at most R_c , only the nodes within R_c from the point N can contribute to the spherical triangle which bounds a spherical triangular hole containing N . Therefore, we only need to consider the Poisson point process constrained on the spherical cap $C(N, R_c)$ which is also a homogeneous Poisson process with intensity λ , where $C(N, R_c)$ denotes the spherical cap centered at point N and the maximum great circle distance between N and points on the spherical cap is R_c . We denote this process as Φ . In addition, $T(x, y, z)$ denotes the property that the point N is inside the spherical triangular hole bounded by the spherical triangle with points x, y, z as vertices. When n_0, n_1, n_2 are points of the process Φ , $T(n_0, n_1, n_2)$ is also used to denote the event that the spherical triangle formed by the nodes n_0, n_1, n_2 bounds a spherical triangular hole containing the point N . In addition, we use $T'(n_0, n_1, n_2)$ to denote the event that the nodes n_0, n_1, n_2 can not form a spherical triangle which bounds a spherical triangular hole containing the point N .

Let $\tau_0 = \tau_0(\Phi)$ be the node in the process Φ which is closest to the point N . There are two cases for the point N to be inside a spherical triangular hole. The first case is that the node τ_0 can contribute to a spherical triangle which bounds a spherical triangular hole containing the point N . The second case is that the node τ_0 can not contribute to any spherical triangle which bounds a spherical triangular hole containing the point N but other three nodes can form a spherical triangle which bounds a spherical triangular hole containing the point N . So the probability that the point N is inside a spherical

triangular hole can be defined as

$$\begin{aligned} p(\lambda) &= \text{P}\{N \text{ is inside a spherical triangular hole}\} \\ &= \text{P}\left\{\bigcup_{\{n_0, n_1, n_2\} \subseteq \Phi} T(n_0, n_1, n_2)\right\} \\ &= \text{P}\left\{\bigcup_{\{n_1, n_2\} \subseteq \Phi \setminus \{\tau_0(\Phi)\}} T(\tau_0, n_1, n_2)\right\} + p_{sec}(\lambda) \end{aligned} \quad (2)$$

where

$$p_{sec}(\lambda) = \text{P}\left\{\bigcup_{\substack{\{n_0, \dots, n_4\} \\ \subseteq \Phi \setminus \{\tau_0(\Phi)\}}} T(n_0, n_1, n_2) \mid T'(\tau_0, n_3, n_4)\right\}$$

denotes the probability of the second case. $p_{sec}(\lambda)$ is generally very small and is obtained by simulations.

B. Analytical lower and upper bounds

As conjectured from Corollary 1, there exist spherical triangular holes only in the case $R_c > R \arccos([3 \cos^2(R_s/R) - 1]/2)$, so we only consider this case. The lower and upper bounds of $p(\lambda)$ are given as follows.

Theorem 1. *When $R_c > R \arccos([3 \cos^2(R_s/R) - 1]/2)$, $p_l(\lambda) < p(\lambda) < p_u(\lambda)$, where*

$$\begin{aligned} p_l(\lambda) &= 2\pi\lambda^2 R^4 \int_{R_s/R}^{\theta_{0u}} \sin \theta_0 d\theta_0 \int_{2\pi - \varphi_m(\theta_0)}^{2\varphi_m(\theta_0)} d\varphi_1 \int_{\theta_0}^{\theta_{1u}(\theta_0, \varphi_1)} \\ &\sin \theta_1 \times e^{-\lambda|C(N, R\theta_0)|} e^{-\lambda|S^+(\theta_0, \varphi_1)|} (1 - e^{-\lambda|S^-(\theta_0, \theta_1, \varphi_1)|}) d\theta_1 \end{aligned} \quad (3)$$

and

$$\begin{aligned} p_u(\lambda) &= 2\pi\lambda^2 R^4 \int_{R_s/R}^{\theta_{0u}} \sin \theta_0 d\theta_0 \int_{2\pi - \varphi_m(\theta_0)}^{2\varphi_m(\theta_0)} d\varphi_1 \int_{\theta_0}^{\theta_{1u}(\theta_0, \varphi_1)} \\ &\sin \theta_1 \times e^{-\lambda|C(N, R\theta_0)|} e^{-\lambda|S^+(\theta_0, \varphi_1)|} (1 - e^{-\lambda|S^-(\theta_0, \theta_1, \varphi_1)|}) d\theta_1 \\ &+ p_{sec}(\lambda) \end{aligned} \quad (4)$$

and $\theta_{0u} = \arccos \sqrt{[1 + 2 \cos(R_c/R)]/3}$

$$\varphi_m(\theta_0) = \begin{cases} \pi & \text{if } \frac{R_s}{R} < \theta_0 \leq \frac{R_c}{2R} \\ \arccos \frac{\cos \frac{R_c}{R} - \cos^2 \theta_0}{\sin^2 \theta_0} & \text{otherwise} \end{cases} \quad (5)$$

$$\theta_{1u}(\theta_0, \varphi_1) = \min\{\theta_{1u1}(\theta_0, \varphi_1), \theta_{1u2}(\theta_0, \varphi_1)\} \quad (6)$$

$$\begin{aligned} \theta_{1u1}(\theta_0, \varphi_1) &= \arccos \frac{\cos(R_c/R)}{\sqrt{1 - \sin^2 \theta_0 \sin^2 \varphi_1}} \\ &+ \arctan(\cos \varphi_1 \tan \theta_0) \end{aligned} \quad (7)$$

$$\begin{aligned} \theta_{1u2}(\theta_0, \varphi_1) &= \arccos \frac{\cos(R_c/R)}{\sqrt{1 - \sin^2 \theta_0 \sin^2(\varphi_1 - \varphi_m(\theta_0))}} \\ &+ \arctan(\cos(\varphi_1 - \varphi_m(\theta_0)) \tan \theta_0) \end{aligned} \quad (8)$$

$$|C(N, R\theta_0)| = 2\pi R^2 (1 - \cos \theta_0) \quad (9)$$

$$|S^+(\theta_0, \varphi_1)| = \int_{2\pi - \varphi_m(\theta_0)}^{\varphi_1} \int_{\theta_0}^{\theta_{1u}(\theta_0, \varphi)} R^2 \sin \theta d\theta d\varphi \quad (10)$$

$$|S^-(\theta_0, \theta_1, \varphi_1)| = \int_{\varphi_{2l}}^{\varphi_m(\theta_0)} \int_{\theta_0}^{\theta_{2u}} R^2 \sin \theta_2 d\theta_2 d\varphi_2 \quad (11)$$

$$\varphi_{2l} = \varphi_1 - \arccos \frac{\cos(R_c/R) - \cos \theta_1 \cos \theta_0}{\sin \theta_1 \sin \theta_0}$$

$$\theta_{2u} = \min\{\theta_{1u1}, \theta_{2u2}\}$$

$$\begin{aligned} \theta_{2u2} &= \arccos \left[\cos(R_c/R) / \sqrt{1 - \sin^2 \theta_0 \sin^2(\varphi_2 - \varphi_1)} \right] \\ &+ \arctan(\cos(\varphi_2 - \varphi_1) \tan \theta_1) \end{aligned}$$

$p_{sec}(\lambda)$ is obtained by simulations¹.

Since the proof is tedious, we only give the main steps of the proof. Please refer to Appendix B for detailed computation.

For the lower bound, we only consider the first case that the closest node τ_0 must contribute to a spherical triangle which bounds a spherical triangular hole containing the point N . The main idea is to first fix the closest node τ_0 , and then sequentially decide the regions where the other two nodes may lie in, and finally do a triple integral.

Using spherical coordinates, we assume the closest node τ_0 lies on $(R, \alpha_0, 0)$. Once the node τ_0 is determined, the other two nodes must lie in the different half spaces: one in $H^+ = \mathbb{R}^+ \times (0, \pi/2) \times (\pi, 2\pi)$ and the other in $H^- = \mathbb{R}^+ \times (0, \pi/2) \times (0, \pi)$. Assume n_1 lies in H^+ and n_2 lies in H^- . Since the great circle distance to τ_0 is at most R_c , n_1 and n_2 must also lie in the spherical cap $C(\tau_0, R_c)$. Furthermore, the great circle distance to the point N is at most R_c and larger than $R\alpha_0$, they should also lie in the region $C(N, R_c) \setminus C(N, R\alpha_0)$. Therefore, n_1 must lie in $H^+ \cap C(\tau_0, R_c) \cap C(N, R_c) \setminus C(N, R\alpha_0)$ and n_2 must lie in $H^- \cap C(\tau_0, R_c) \cap C(N, R_c) \setminus C(N, R\alpha_0)$. In addition, considering the great circle distance between n_1 and n_2 should be at most R_c and the point N should be inside the spherical triangle formed by τ_0 , n_1 and n_2 , n_1 must lie in the shadow region A^+ shown in Figures 3 or 4 under different situations. In the case $R \arccos([3 \cos^2(R_s/R) - 1]/2) < R_c \leq 2R_s$ or in the case $R_c > 2R_s, R_c/(2R) < \alpha_0 \leq \arccos \sqrt{[1 + 2 \cos(R_c/R)]/3}$, $A^+ = H^+ \cap C(\tau_0, R_c) \cap C(N, R_c) \setminus C(N, R\alpha_0) \cap C(M_2, R_c)$, shown in Figure 3. M_1 and M_2 are two intersection points between bases of spherical caps $C(N, R\alpha_0)$ and $C(\tau_0, R_c)$. In the case $R_c > 2R_s, R_s/R < \alpha_0 \leq R_c/(2R)$, $A^+ = H^+ \cap C(\tau_0, R_c) \cap C(N, R_c) \setminus C(N, R\alpha_0) \cap C(M, R_c)$, as in Figure 4, where M is one intersection point between base of spherical caps $C(N, R\alpha_0)$ and the plane xOz .

Ordering the nodes in A^+ by increasing azimuth angle so that $\tau_1 = (R, \theta_1, \varphi_1)$ has the smallest azimuth angle φ_1 . And assume the nodes τ_0 , τ_1 and another node $\tau_2 \in H^- \cap C(\tau_0, R_c) \cap C(N, R_c) \setminus C(N, R\alpha_0)$ can form a spherical triangle which bounds a spherical triangular hole containing the point N , then τ_2 must lie to the right of the great circle passing through τ_1 and N , denoted by $H^+(\varphi_1)$ which contains all points with azimuth angle $\varphi \in (\varphi_1 - \pi, \varphi_1)$. In addition, the great circle distance to τ_1 is no larger than R_c , so the node τ_2 must lie in the region S^- , as illustrated in Figures 4 and 5.

$$\begin{aligned} S^-(\tau_0, \tau_1) &= S^-(\alpha_0, \theta_1, \varphi_1) = H^- \cap C(\tau_0, R_c) \\ &\cap C(N, R_c) \setminus C(N, R\theta_0) \cap H^+(\varphi_1) \cap C(\tau_1, R_c) \end{aligned}$$

¹It is a non-trivial task to derive a closed-form expression for $p_{sec}(\lambda)$. Furthermore, we find that it is much less than the closed-form part in upper bound $p_u(\lambda)$ and it has little impact on the derived bound. We thus get it by simulations.

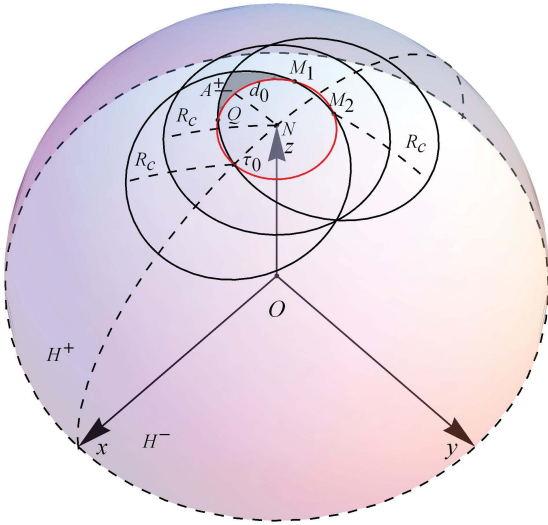


Fig. 3. Illustration of region A^+ in the case $R \arccos([3 \cos^2(R_s/R) - 1]/2) < R_c \leq 2R_s$ or in the case $R_c > 2R_s, R_c/(2R) < \alpha_0 \leq \arccos \sqrt{[1 + 2 \cos(R_c/R)]/3}$

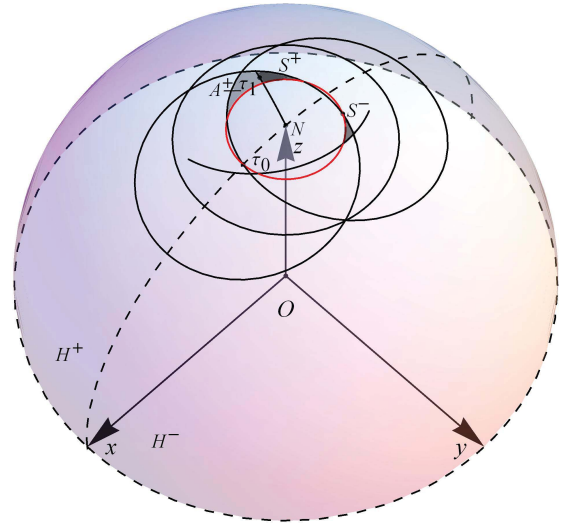


Fig. 5. Illustration of regions S^+ and S^- in the case $R \arccos([3 \cos^2(R_s/R) - 1]/2) < R_c \leq 2R_s$

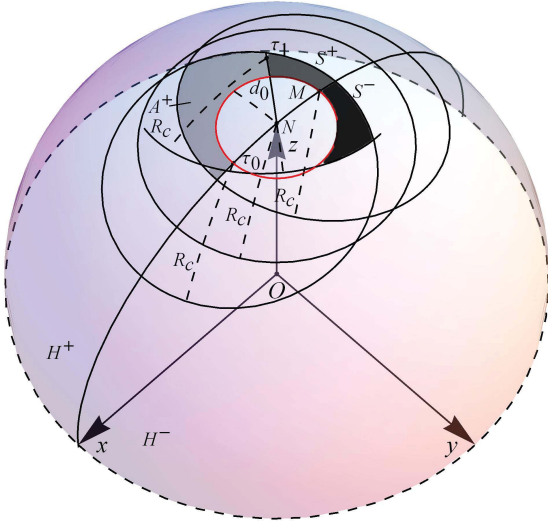


Fig. 4. Illustration of regions A^+, S^+ and S^- in the case $R_c > 2R_s, R_s/R < \alpha_0 \leq R_c/(2R)$

Assume only τ_0, τ_1 and nodes in $S^-(\tau_0, \tau_1)$ can contribute to the spherical triangle which bounds a spherical triangular hole containing the point N , we can get a lower bound of the probability that the point N is inside a spherical triangular hole. It is a lower bound because it is possible that τ_1 can not contribute to a spherical triangle which bounds a spherical triangular hole containing point N , but some other nodes with higher azimuth angles in the region A^+ can contribute to such a spherical triangle. For example, in Figure 6, if there is no node in S^- but there are some nodes in S'^- , then τ_1 can not contribute to any spherical triangle which bounds a spherical triangular hole containing point N , but τ'_1 can form such a spherical triangle with τ_0 and another node in S'^- .

Next we will prove the upper bound. As discussed in Section IV-A, there are two cases for the point N being inside a spherical triangular hole. As for the second case that the

closest node τ_0 can not but some other nodes can contribute to a spherical triangle which bounds a spherical triangular hole containing the point N , it is not easy to obtain a closed-form expression for such probability, so we get it by simulations. Simulation results show that this probability is less than 0.16% whenever $R_c \leq 3R_s$ with any intensity λ . So we still focus on the probability of the first case.

Still consider the nodes in A^+ , each node (R, θ, φ) corresponds to an area $|S^-(\alpha_0, \theta, \varphi)|$. The higher is the area $|S^-(\alpha_0, \theta, \varphi)|$, the higher is the probability that there is at least one node in $S^-(\alpha_0, \theta, \varphi)$, consequently the probability of the first case will be higher. It can be seen from Figures 4 and 5 that the closer to α_0 is θ and the closer to φ_1 is φ , the higher is the area $|S^-(\alpha_0, \theta, \varphi)|$. So the largest area $|S^-(\alpha_0, \theta, \varphi)|$ is $|S^-(\alpha_0, \alpha_0, \varphi_1)|$. Based on that, the upper bound can be derived.

As can be seen, the expression for lower bound is closed-form, while the expression for upper bound is not exactly closed-form since it includes a non-analytical part $p_{sec}(\lambda)$. As for lower bound and the closed-form part for upper bound, we use numerical integration to approximate the triple integrals. As for $p_{sec}(\lambda)$, we get it by simulations since it is very small, it has little impact on the derived bound.

C. Asymptotic lower and upper bounds

Intuitively, when $R \rightarrow \infty$, the case on sphere should be the same as that in plane, which is shown in the following theorem.

Theorem 2. When $R \rightarrow \infty$ and $R_c > \sqrt{3}R_s$, lower and upper bounds in (3) and (4) become

$$p'_l(\lambda) = 2\pi\lambda^2 \int_{R_s}^{R_c/\sqrt{3}} r_0 dr_0 \int_{\varphi_l(r_0)}^{\varphi_u(r_0)} d\varphi'_1 \int_{r_0}^{R_1(r_0, \varphi'_1)} e^{-\lambda\pi r_0^2} \times e^{-\lambda|S^+(r_0, \varphi'_1)|} (1 - e^{-\lambda|S^-(r_0, r_1, \varphi'_1)|}) r_1 dr_1 \quad (12)$$

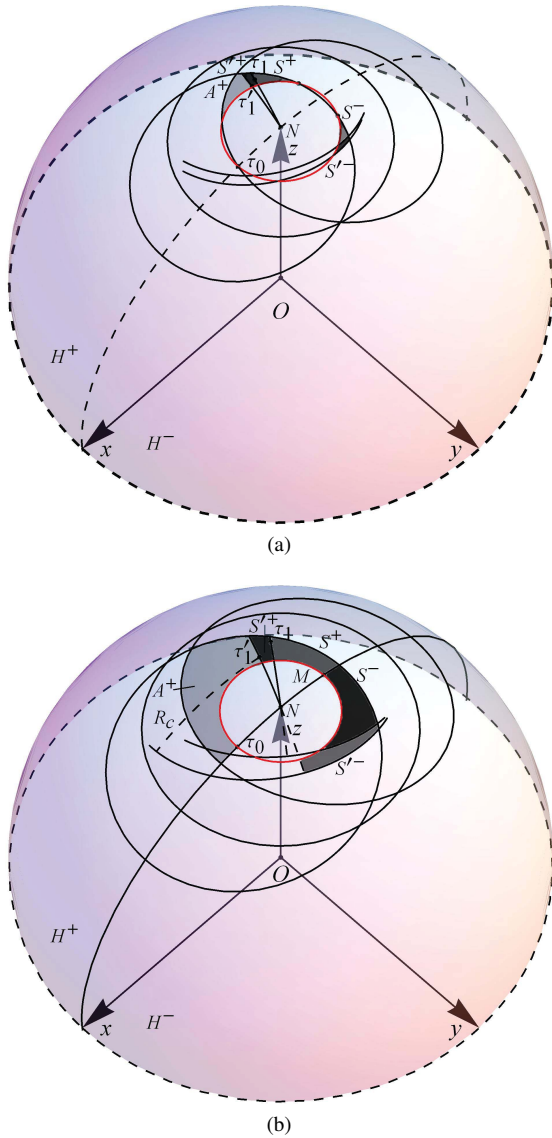


Fig. 6. Illustrations of regions S'^+ and S'^- (a) in the case $R \arccos([3 \cos^2(R_s/R) - 1]/2) < R_c \leq 2R_s$ or in the case $R_c > 2R_s, R_c/(2R) < \alpha_0 \leq \arccos \sqrt{[1 + 2 \cos(R_c/R)]/3}$; (b) in the case $R_c > 2R_s, R_s/R < \alpha_0 \leq R_c/(2R)$

and

$$p'_u(\lambda) = 2\pi\lambda^2 \int_{R_s}^{R_c/\sqrt{3}} r_0 dr_0 \int_{\varphi_l(r_0)}^{\varphi_u(r_0)} d\varphi'_1 \int_{r_0}^{R_1(r_0, \varphi'_1)} r dr d\varphi' \quad (13)$$

$$e^{-\lambda\pi r_0^2} \times e^{-\lambda|S^+(r_0, \varphi'_1)|} (1 - e^{-\lambda|S^-(r_0, r_0, \varphi'_1)|}) r_1 dr_1 + p_{sec}(\lambda)$$

where

$$\varphi_l(r_0) = \begin{cases} 0 & \text{if } R_s < r_0 \leq R_c/2 \\ 2 \arccos(R_c/(2r_0)) & \text{otherwise} \end{cases} \quad (14)$$

$$\varphi_u(r_0) = \begin{cases} \pi & \text{if } R_s < r_0 \leq R_c/2 \\ \pi - 4 \arccos \frac{R_c}{2r_0} & \text{otherwise} \end{cases} \quad (15)$$

$$R_1(r_0, \varphi'_1) = \min(\sqrt{R_c^2 - r_0^2 \sin^2 \varphi'_1} - r_0 \cos \varphi'_1, \quad (16)$$

$$\sqrt{R_c^2 - r_0^2 \sin^2(\varphi'_1 + \varphi_l(r_0))} + r_0 \cos(\varphi'_1 + \varphi_l(r_0)))$$

$$|S^+(r_0, \varphi'_1)| = \int_{\varphi_l(r_0)}^{\varphi'_1} \int_{r_0}^{R_1(r_0, \varphi'_1)} r dr d\varphi' \quad (17)$$

$$|S^-(r_0, r_1, \varphi'_1)| = \int_{\varphi'_{2l}}^{-\varphi_l(r_0)} \int_{r_0}^{R_2(r_0, r_1, \varphi'_1, \varphi'_2)} r_2 dr_2 d\varphi'_2 \quad (18)$$

$$\varphi'_{2l} = \varphi'_1 - \arccos((r_0^2 + r_1^2 - R_c^2)/(2r_0r_1))$$

$$R_2(r_0, r_1, \varphi'_1, \varphi'_2) = \min(\sqrt{R_c^2 - r_0^2 \sin^2 \varphi'_2} - r_0 \cos \varphi'_2, \quad (19)$$

$$\sqrt{R_c^2 - r_1^2 \sin^2(\varphi'_2 - \varphi'_1)} + r_1 \cos(\varphi'_2 - \varphi'_1))$$

$p_{sec}(\lambda)$ is obtained by simulations.

Proof: Please refer to Appendix C. ■

Comparing (12) and (13) to the results in the paper [25], we can find that they are the same, which is quite logical since when $R \rightarrow \infty$ the local of each node can be considered to be planar.

V. SIMULATIONS AND PERFORMANCE EVALUATION

In this section, simulation settings are first given. Then simulation results are compared with analytical lower and upper bounds under different settings of R_s, R_c, R .

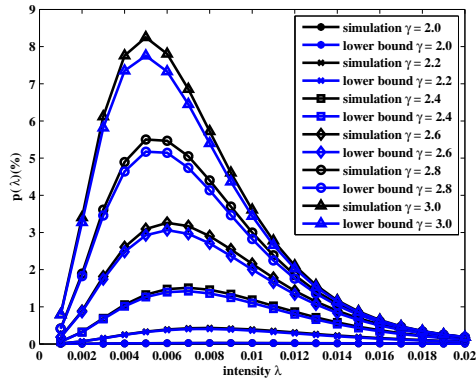
A. Simulation settings

A sphere centered at the origin with radius R is considered in the simulations. The probability of the point with spherical coordinate $(R, 0, 0)$ being inside a spherical triangular hole is computed. Sensors are randomly distributed on the sphere according to a homogeneous Poisson point process with intensity λ . The sensing radius R_s of each node is set to be 10 meters and communication radius R_c is chosen from 20 to 30 meters with interval of 2 meters. Let $\gamma = R_c/R_s$, then γ ranges from 2 to 3 with interval of 0.2. In addition, λ is selected from 0.001 to 0.020 with interval of 0.001. For each pair of (λ, γ) , 10^7 simulations are run to check whether the point with spherical coordinate $(R, 0, 0)$ is inside a spherical triangular hole.

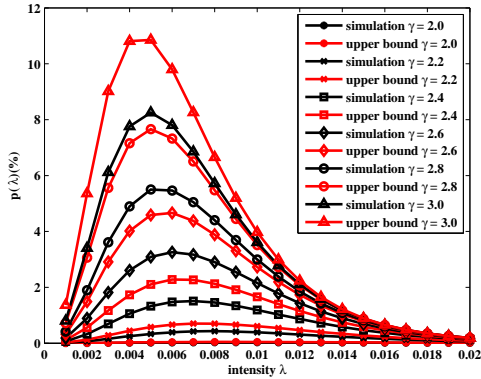
B. Impact of R_s and R_c

As illustrated in Section III, $R_s \ll R$ and $R_c \ll R$, here we fix $R = 10R_s$, choose R_s to be 10 meters and R_c to be 20 to 30 meters with interval of 2 meters, to analyse the impact of R_s and R_c on the probability of any point being inside a spherical triangular hole. Under this configuration, the probability $p(\lambda)$ obtained by simulations is presented with the lower and upper bounds in Figure 7(a) and 7(b) respectively. Note that the upper bounds contain the simulation results for $p_{sec}(\lambda)$ which are shown in Figure 7(c).

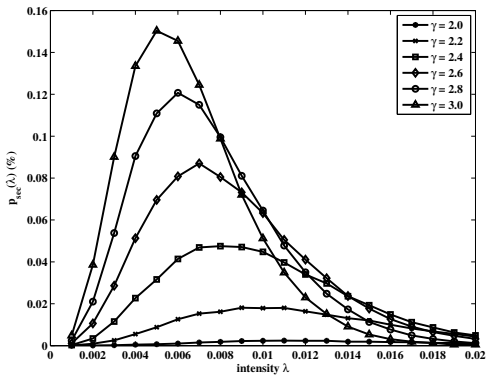
It can be seen that for any value of γ , $p(\lambda)$ has a maximum at a threshold value λ_c of the intensity. As a matter of fact, for $\lambda \leq \lambda_c$, the number of nodes is small. Consequently the probability of any point being inside a spherical triangular hole is relatively small too. With the increase of λ , the connectivity



(a)



(b)



(c)

Fig. 7. Proportion of the area of spherical triangular holes under $R = 10R_s$. (a) simulation results and lower bounds; (b) simulation results and upper bounds; (c) simulation results for $p_{sec}(\lambda)$

between nodes becomes stronger. As a result, the probability of any point being inside a spherical triangular hole increases. However, when the intensity reaches the threshold value, the probability is up to its maximum. $p(\lambda)$ decreases for $\lambda \geq \lambda_c$. The simulations also show that λ_c decreases with the increase of γ .

On the other hand, it can be seen from Figure 7(a) and 7(b) that for a fixed intensity λ , $p(\lambda)$ increases with the increases of γ . That is because when R_s is fixed, the larger R_c is, the higher is the probability of each spherical triangle containing

a coverage hole.

Furthermore, the maximum probability increases quickly with γ ranging from 2.0 to 3.0. These results can also provide some insights for planning of WSNs, which will be discussed in Section V-D.

Finally, it can be found in Figure 7(a) that the probability obtained by simulation is very well consistent with the lower bound. The maximum difference between them is about 0.5%. Figure 7(b) shows that probability obtained by simulation is also consistent with the upper bound. The maximum difference between them is about 3%.

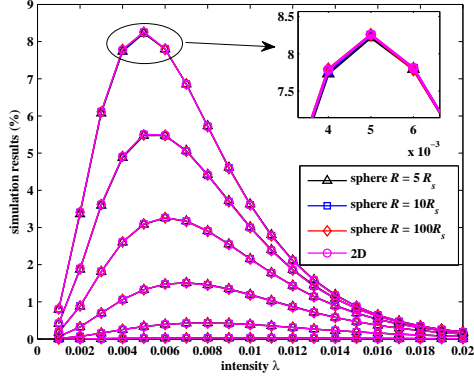
C. Impact of R

Although we assume $R_s \ll R$ and $R_c \ll R$, to better understand the impact of R on the probability of any point being inside a spherical triangular hole, we choose R to be $5R_s, 10R_s$ and $100R_s$. In these cases, R_s is still 10 meters and R_c is from 20 to 30 meters with interval of 2 meters. In addition, we also want to know the difference of the probability under spherical and 2D planar cases. Therefore, simulation results, lower and upper bounds of the probability under spheres with radii $5R_s, 10R_s, 100R_s$ and 2D plane are shown in Figure 8(a), 8(b) and 8(c) respectively. Simulation results for $p_{sec}(\lambda)$ under spheres with radii $5R_s, 10R_s, 100R_s$ and 2D plane are shown in Figure 9. From Figure 9, we can find that $p_{sec}(\lambda)$ is less than 0.16% under any intensity in these cases.

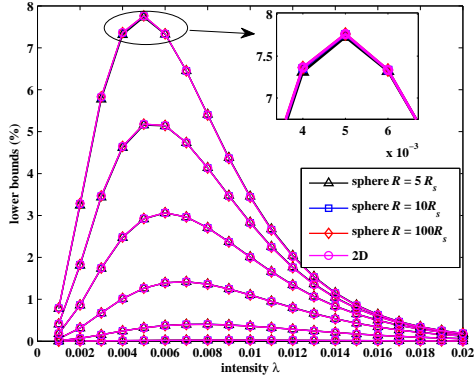
It can be seen from Figure 8 that simulations results, lower and upper bounds under spheres with radii $5R_s, 10R_s, 100R_s$ and 2D plane are very close with each other. More precisely, the maximum difference of simulations results under spheres with radii $5R_s$ and $10R_s$ is about 0.045%, which is about 0.06% under spheres with radii $5R_s$ and $100R_s$ and is about 0.03% under spheres with radii $10R_s$ and $100R_s$. In addition, the maximum differences of simulation results between 2D planar case and spherical cases with radii $5R_s, 10R_s, 100R_s$ are 0.05%, 0.03% and 0.02% respectively. It means the larger the radius of sphere is, the more closer are the simulation results under sphere and 2D plane, it is because the larger the radius of sphere is, the more likely of the local of each node on the sphere to be planar.

With respect to lower and upper bounds, it is found that under any two spheres with radii $5R_s, 10R_s, 100R_s$, the maximum difference of lower and upper bounds are 0.06% and 0.12% respectively. Furthermore, under spheres with radii $5R_s, 10R_s, 100R_s$ and 2D plane, the maximum difference of lower bounds is also 0.06%, and that of upper bounds is also 0.12%. More importantly, under sphere with radius $100R_s$ and 2D plane, the maximum difference of lower bounds is 5×10^{-6} and that of upper bounds is 2.5×10^{-5} . It means the probabilities under cases of sphere with radius $100R_s$ and 2D plane are nearly the same, which is quite logical since when the radius of sphere is much more larger than the sensing radius of any node, the local of any node can be considered to be planar.

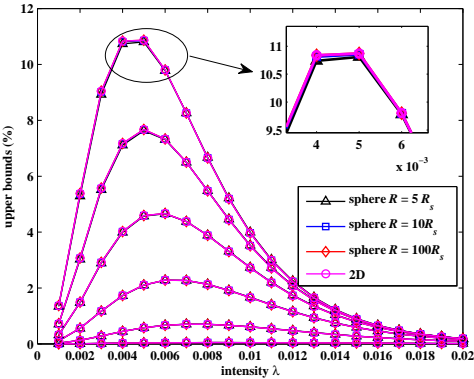
It can be further found that under above cases, the maximum differences of simulation results, lower and upper bounds



(a)



(b)



(c)

Fig. 8. Comparison of the proportion of the area of spherical triangular holes (a) comparison of simulation results; (b) comparison of lower bounds; (c) comparison of upper bounds

are all so small that they can be neglected. Consequently, it also means that the radius of sphere has little impact on the probability of any point on the sphere to be inside a spherical triangular hole.

D. Discussions on applications

In this paper, we only consider spherical triangular holes, for non-spherical triangular holes, we assume they can be detected and covered by additional nodes. Under this assumption, our

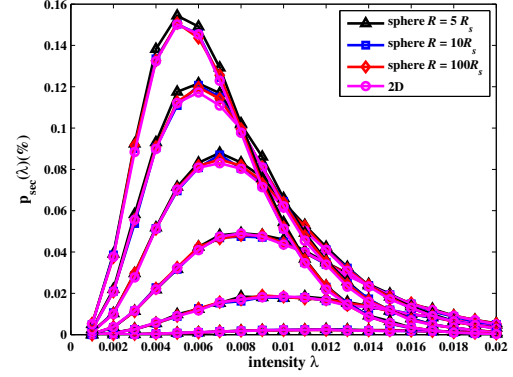


Fig. 9. Simulation results for $p_{sec}(\lambda)$

analytical results can be used for planning of WSNs. For example, a WSN is used to monitor a mountain and the ratio $\gamma = 2$, according to the analytical upper bounds, we can see that the maximum proportion of the area of spherical triangular holes under $\gamma = 2$ is about 0.06 %, which can be neglected. It means that as long as the surface of mountain can be spherically triangulated by nodes, we can say the mountain is covered. But if $\gamma = 3$ and at least 95% of the surface of the mountain should be covered, then it means that the proportion of the area of spherical triangular holes can be at most 5%. From the analytical upper bounds of $\gamma = 3$, it can be seen that when the intensity $\lambda = 0.009$, the upper bound is about 5%, so in order to cover at least 95% of the mountain, the intensity of nodes should be larger than 0.009.

VI. CONCLUSIONS

This paper studied the accuracy of homology-based coverage hole detection for wireless sensor networks on sphere. First, the case when Rips complex may miss coverage holes was identified. It was found that a hole missed by Rips complex must be bounded by a spherical triangle and a formal definition of spherical triangular hole was given. Then we chose the proportion of the area of spherical triangular holes as a metric to evaluate the accuracy. Closed-form expressions for lower and upper bounds were derived. Asymptotic lower and upper bounds are also investigated when the radius of sphere tends to infinity. Simulation results are well consistent with the derived lower and upper bounds, with maximum differences of 0.5% and 3% respectively. In addition, simulation results also show that the radius of sphere has little impact on the accuracy as long as it is much larger than communication and sensing radii of each sensor. This means that our results may be potentially applied to more general 3D surfaces although the results are derived on sphere. This problem will be investigated in our future work.

APPENDIX A PROOF OF LEMMA 1

Proof: The second inclusion is trivial because for any k -simplex $[v_0, v_1, \dots, v_k] \in \check{C}_{R_s}^{(2)}(\mathcal{V})$, it means the sensing ranges of these nodes have a common intersection, so the

pairwise distance $d(v_i, v_j) \leq 2R_s$ for all $0 \leq i < j \leq k$, which means $[v_0, v_1, \dots, v_k] \in \mathcal{R}_{2R_s}^{(2)}(\mathcal{V})$.

As for the first inclusion, it is clear that $\mathcal{R}_{R_c}^{(2)}(\mathcal{V})$ and $\check{\mathcal{C}}_{R_s}^{(2)}(\mathcal{V})$ contain the same 0-simplices. It is also easy to see that all 1-simplices in $\mathcal{R}_{R_c}^{(2)}(\mathcal{V})$ must also be in $\check{\mathcal{C}}_{R_s}^{(2)}(\mathcal{V})$ since for any 1-simplex $[v_i, v_j]$ with distance $d(v_i, v_j) \leq R_c \leq R \arccos([3 \cos^2(R_s/R) - 1]/2) < R \arccos(2 \cos^2(R_s/R) - 1) = 2R_s$, it means that the sensing ranges of the two nodes have a common intersection. So we only need to prove that all 2-simplices in $\mathcal{R}_{R_c}^{(2)}(\mathcal{V})$ must be in $\check{\mathcal{C}}_{R_s}^{(2)}(\mathcal{V})$. It is equivalent to say that for any three nodes with pairwise great circle distance no larger than R_c , their sensing ranges must have a common intersection.

Assume a 2-simplex $[v_0, v_1, v_2] \in \mathcal{R}_{R_c}^{(2)}(\mathcal{V})$, then the three nodes v_0, v_1 and v_2 must determine a plane α . We consider the spherical cap on \mathbb{S}^2 cut off by the plane α . Since $R_c < R$, the spherical cap must be on a hemisphere. It is easy to see that the intersection of the plane α and sphere \mathbb{S}^2 is a circle c . Let O_1 be the center of circle c , O be the center of \mathbb{S}^2 , P be the intersection of line OO_1 and \mathbb{S}^2 .

Using spherical coordinates, we assume the point P has a spherical coordinate $(R, 0, 0)$. P may be inside² or outside the spherical triangle $v_0v_1v_2$, which is shown in Figure 10(a) and 10(b) respectively.

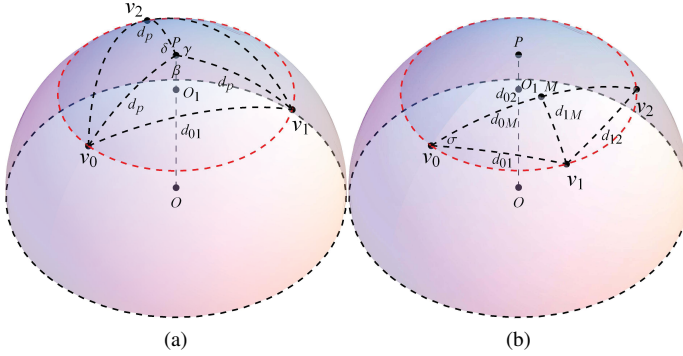


Fig. 10. Illustrations of P and spherical triangle $v_0v_1v_2$: (a) P is inside the spherical triangle $v_0v_1v_2$; (b) P is outside the spherical triangle $v_0v_1v_2$.

It can be seen that P has the same great circle distance to v_0, v_1 and v_2 , denoted by d_p . If P is inside the spherical triangle $v_0v_1v_2$, as shown in Figure 10(a), then we can prove $d_p \leq R_s$. Since P lying inside the spherical triangle $v_0v_1v_2$ means $\beta + \gamma + \delta = 2\pi$, there must be one angle no smaller than $2\pi/3$. Without loss of generality, assume $\beta \geq 2\pi/3$. According to the spherical law of cosines, we have $\cos(\beta) = \frac{\cos(d_{01}/R) - \cos^2(d_p/R)}{\sin^2(d_p/R)} \leq -1/2 \Rightarrow \cos(d_{01}/R) \leq [3 \cos^2(d_p/R) - 1]/2$. In addition, $d_{01} \leq R_c \leq R \arccos([3 \cos^2(R_s/R) - 1]/2) \Rightarrow \cos(d_{01}/R) \geq [3 \cos^2(R_s/R) - 1]/2$, and $0 < d_{01}/R, d_p/R < \pi/2$, so we have $[3 \cos^2(R_s/R) - 1]/2 \leq [3 \cos^2(d_p/R) - 1]/2 \Rightarrow d_p \leq R_s$, which means the point P is a common intersection of sensing ranges of v_0, v_1 and v_2 , so $[v_0, v_1, v_2] \in \check{\mathcal{C}}_{R_s}^{(2)}(\mathcal{V})$.

²It also includes the case that P is on one arc of the spherical triangle $v_0v_1v_2$.

If P is outside the spherical triangle $v_0v_1v_2$, as shown in Figure 10(b), it indicates that the spherical triangle $v_0v_1v_2$ must be contained in half of the spherical cap. Assume v_0, v_1 and v_2 have spherical coordinates $(R, \theta, \varphi_0), (R, \theta, \varphi_1)$ and (R, θ, φ_2) , where $\theta \in (0, \pi/2), \varphi_0 < \varphi_1 < \varphi_2$, then we have $\varphi_1 - \varphi_0, \varphi_2 - \varphi_1, \varphi_2 - \varphi_0 \in (0, \pi)$. Using d_{01}, d_{12}, d_{02} to denote the pairwise great circle distances between v_0, v_1, v_2 , then according to the spherical law of cosines, we have

$$\cos(d_{01}/R) = \cos^2 \theta + \sin^2 \theta \cos(\varphi_1 - \varphi_0) \quad (19)$$

$$\cos(d_{12}/R) = \cos^2 \theta + \sin^2 \theta \cos(\varphi_2 - \varphi_1) \quad (20)$$

$$\cos(d_{02}/R) = \cos^2 \theta + \sin^2 \theta \cos(\varphi_2 - \varphi_0) \quad (21)$$

In addition, we use σ to denote the angle between two arcs $\widehat{v_0v_1}$ and $\widehat{v_0v_2}$, M to denote the middle point of the arc $\widehat{v_0v_2}$ and d_{0M}, d_{1M} to denote great circle distances between v_0, v_1 and M . It can be seen $d_{0M} = d_{02}/2$. Similarly, we have

$$\cos \sigma = \frac{\cos(d_{12}/R) - \cos(d_{01}/R) \cos(d_{02}/R)}{\sin(d_{01}/R) \sin(d_{02}/R)} \quad (22)$$

$$\cos \frac{d_{1M}}{R} = \cos \frac{d_{01}}{R} \cos \frac{d_{0M}}{2R} + \sin \frac{d_{01}}{R} \cos \frac{d_{0M}}{2R} \cos \sigma \quad (23)$$

From (22) and (23), we can obtain

$$\cos \frac{d_{1M}}{R} = \frac{\cos(d_{01}/R) + \cos(d_{12}/R)}{2 \cos(d_{02}/(2R))} \quad (24)$$

Consequently

$$\cos \frac{d_{1M}}{R} - \cos \frac{d_{0M}}{R} = \frac{\cos \frac{d_{01}}{R} + \cos \frac{d_{12}}{R} - \cos \frac{d_{02}}{R} - 1}{2 \cos(d_{02}/(2R))} \quad (25)$$

From (19), (20), (21) and (25), we get

$$\cos \frac{d_{1M}}{R} - \cos \frac{d_{0M}}{R} = \frac{\sin^2 \theta \cos \frac{\varphi_2 - \varphi_0}{2} \sin \frac{\varphi_1 - \varphi_0}{2} \sin \frac{\varphi_2 - \varphi_1}{2}}{\cos \frac{d_{02}}{2R}} \quad (26)$$

Since $0 < \varphi_1 - \varphi_0, \varphi_2 - \varphi_1, \varphi_2 - \varphi_0 < \pi$ and $0 < d_{1M}/R, d_{0M}/R, d_{02}/R < \pi/2$, it can be obtained from (26) $d_{1M} < d_{0M} \leq R_c/2 < R_s$, which means the point M is a common intersection of the sensing ranges of v_0, v_1 and v_2 , so $[v_0, v_1, v_2] \in \check{\mathcal{C}}_{R_s}^{(2)}(\mathcal{V})$. It means all 2-simplices in $\mathcal{R}_{R_c}^{(2)}(\mathcal{V})$ must be in $\check{\mathcal{C}}_{R_s}^{(2)}(\mathcal{V})$. Consequently the first inclusion is proved. ■

APPENDIX B PROOF OF THEOREM 1

Proof: We first prove the lower bound. It can be obtained from (2) that

$$p(\lambda) > P\left\{ \bigcup_{\{n_1, n_2\} \subseteq \Phi \setminus \{\tau_0(\Phi)\}} T(\tau_0, n_1, n_2) \right\}$$

So for the lower bound, we only consider the first case that the closest node τ_0 must contribute to a spherical triangle which bounds a spherical triangular hole containing the point N .

Using spherical coordinates, we assume the closest node τ_0 lies on $(R, \alpha_0, 0)$ and use $|S|$ to denote the area of the set S , then we can get the distribution of α_0 as

$$F_{\alpha_0}(\theta_0) = P(\alpha_0 \leq \theta_0) = 1 - e^{-\lambda |C(N, R\theta_0)|} \quad (27)$$

since the event $\alpha_0 > \theta_0$ means that the spherical cap $C(N, R\theta_0)$ does not contain any nodes from the process, which is given by the void probability $e^{-\lambda|C(N, R\theta_0)|}$. Furthermore, $|C(N, R\theta_0)|$ can be given as

$$|C(N, R\theta_0)| = \int_0^{\theta_0} \int_0^{2\pi} R^2 \sin \theta d\varphi d\theta = 2\pi R^2 (1 - \cos \theta_0) \quad (28)$$

From (27) and (28), we can get the density of τ_0

$$F_{\alpha_0}(d\theta_0) = 2\pi\lambda R^2 \sin \theta_0 e^{-\lambda|C(N, R\theta_0)|} d\theta_0 \quad (29)$$

The integration range for θ_0 can be easily obtained. According to Lemma 4, we have $R_s < R\theta_0 \leq R \arccos \sqrt{[1 + 2 \cos(R_c/R)]/3}$, so $R_s/R < \theta_0 \leq \theta_{0u} = \arccos \sqrt{[1 + 2 \cos(R_c/R)]/3}$.

Therefore the probability of the first case can be given as

$$\begin{aligned} & \mathbb{P}\left\{ \bigcup_{\{n_1, n_2\} \subseteq \Phi \setminus \{\tau_0(\Phi)\}} T(\tau_0, n_1, n_2) \right\} \\ &= \int_{R_s/R}^{\theta_{0u}} \mathbb{P}\left\{ \bigcup_{\{n_1, n_2\} \subseteq \Phi'_{\theta_0}} T((R, \theta_0, 0), n_1, n_2) \right\} F_{\alpha_0}(d\theta_0) \end{aligned} \quad (30)$$

where Φ'_{θ_0} is the restriction of Φ in $C(N, R_c) \setminus C(N, R\theta_0)$.

Once the node τ_0 is determined, a second node τ_1 must lie in the shadow region A^+ shown in Figures 3 or 4, and a third node τ_2 must lie in the region S^- shown in Figures 4 or 5, as illustrated in Section IV-B. The node $\tau_1 = (R, \theta_1, \varphi_1)$ is assumed to have the smallest azimuth angle in A^+ , which means that there should be no nodes with a azimuth angle less than φ_1 in A^+ , that is to say no nodes are in the region

$$S^+(\tau_0, \tau_1) = S^+(\alpha_0, \varphi_1) = A^+ \cap H^+(\varphi_1)$$

Since the intensity measure of the Poisson point process in spherical coordinates is $\lambda R^2 \sin \theta d\theta d\varphi$, the density F_{τ_1} of τ_1 can be given as

$$F_{\tau_1}(d\theta_1, d\varphi_1) = \lambda R^2 \sin \theta_1 e^{-\lambda|S^+(\alpha_0, \varphi_1)|} d\theta_1 d\varphi_1 \quad (31)$$

Then we derive the integration domain $D(\alpha_0)$ with respect to parameters (θ_1, φ_1) . Consider the case shown in Figure 3, assume the point M_2 has the spherical coordinate (R, α_0, φ_m) , $\varphi_m \in (0, \pi)$. Since the great circle distance between τ_0 and M_2 is R_c , then according to the spherical law of cosines, we have $\cos(R_c/R) = \cos^2 \alpha_0 + \sin^2 \alpha_0 \cos \varphi_m \Rightarrow \varphi_m(\alpha_0) = \arccos[(\cos(R_c/R) - \cos^2 \alpha_0)/(\sin^2 \alpha_0)]$. It can be seen that points M_1 and Q have the spherical coordinates $(R, \alpha_0, 2\pi - \varphi_m(\alpha_0))$ and $(R, \alpha_0, 2\varphi_m(\alpha_0))$ respectively, where Q is one intersection point between bases of spherical caps $C(N, R\alpha_0)$ and $C(M_2, R_c)$. Thus the integration range for φ_1 is $[2\pi - \varphi_m(\alpha_0), 2\varphi_m(\alpha_0)]$. In addition, assume any point with great circle distance R_c to τ_0 has the spherical coordinate (R, θ_t, φ_t) , still using the spherical law of cosines, we have $\cos(R_c/R) = \cos \alpha_0 \cos \theta_t + \sin \alpha_0 \sin \theta_t \cos \varphi_t \Rightarrow \theta_t(\alpha_0, \varphi_t) = \arccos[\cos(R_c/R)/\sqrt{1 - \sin^2 \alpha_0 \sin^2 \varphi_t}] + \arctan(\cos \varphi_t \tan \alpha_0)$. Similarly, assume any point with great circle distance R_c to M_2 has the spherical coordinate $(R, \theta'_t, \varphi'_t)$, we can obtain $\theta'_t(\alpha_0, \varphi'_t) = \arccos[\cos(R_c/R)/\sqrt{1 - \sin^2 \alpha_0 \sin^2(\varphi'_t - \varphi_m(\alpha_0))}] +$

$\arctan(\cos(\varphi'_t - \varphi_m(\alpha_0)) \tan \alpha_0)$. Then the integration range for θ_1 is $[\alpha_0, \theta_{1u}(\alpha_0, \varphi_1)]$, where $\theta_{1u}(\alpha_0, \varphi_1) = \min\{\theta_{1u1}(\alpha_0, \varphi_1), \theta_{1u2}(\alpha_0, \varphi_1)\}$, $\theta_{1u1}(\alpha_0, \varphi_1) = \theta_t(\alpha_0, \varphi_1)$, $\theta_{1u2}(\alpha_0, \varphi_1) = \theta'_t(\alpha_0, \varphi_1)$.

Consider the case shown in Figure 4, the derivation of the integration domain $D(\alpha_0)$ is the same as the case shown in Figure 3. In this case, the point M has the spherical coordinate (R, α_0, π) , and the integration range for φ_1 is $[\pi, 2\pi]$. If we define

$$\varphi_m(\alpha_0) = \begin{cases} \pi & \text{if } \frac{R_s}{R} < \alpha_0 \leq \frac{R_c}{2R} \\ \arccos \frac{\cos \frac{R_c}{R} - \cos^2 \alpha_0}{\sin^2 \alpha_0} & \text{otherwise} \end{cases}$$

then the two cases can be regarded as the same in terms of the integration domain $D(\alpha_0)$.

Furthermore, $|S^+(\alpha_0, \varphi_1)|$ can be expressed as

$$|S^+(\alpha_0, \varphi_1)| = \int_{2\pi - \varphi_m(\alpha_0)}^{\varphi_1} \int_{\alpha_0}^{\theta_{1u}(\alpha_0, \varphi_1)} R^2 \sin \theta d\theta d\varphi$$

As illustrated in Section IV-B, assume only τ_0, τ_1 and nodes in $S^-(\tau_0, \tau_1)$ can contribute to the spherical triangle which bounds a spherical triangular hole containing the point N , we can get a lower bound of the probability that the point N is inside a spherical triangular hole. Based on the assumption, we have

$$\begin{aligned} & \mathbb{P}\left\{ \bigcup_{\{n_1, n_2\} \subseteq \Phi'_{\theta_0}} T((R, \theta_0, 0), n_1, n_2) \right\} \\ &> \mathbb{P}\left\{ \bigcup_{n_2 \subseteq \Phi'_{\theta_0} \cap S^-(\tau_0, \tau_1)} T((R, \theta_0, 0), \tau_1, n_2) \right\} \\ &= \iint_{D(\theta_0)} \mathbb{P}\left\{ \bigcup_{\substack{n_2 \subseteq \Phi'_{\theta_0} \cap \\ S^-(\theta_0, \theta_1, \varphi_1)}} T((R, \theta_0, 0), (R, \theta_1, \varphi_1), n_2) \right\} \\ & \quad F_{\tau_1}(d\theta_1, d\varphi_1) \\ &= \iint_{D(\theta_0)} \mathbb{P}\{\Phi'_{\theta_0}(S^-(\theta_0, \theta_1, \varphi_1)) > 0\} F_{\tau_1}(d\theta_1, d\varphi_1) \\ &= \iint_{D(\theta_0)} (1 - e^{-\lambda|S^-(\theta_0, \theta_1, \varphi_1)|}) F_{\tau_1}(d\theta_1, d\varphi_1) \end{aligned} \quad (32)$$

where $|S^-(\theta_0, \theta_1, \varphi_1)|$ can be expressed as

$$|S^-(\theta_0, \theta_1, \varphi_1)| = \int_{\varphi_{2l}}^{\varphi_m} \int_{\theta_0}^{\theta_{2u}} R^2 \sin \theta_2 d\theta_2 d\varphi_2$$

and

$$\begin{aligned} \varphi_{2l} &= \varphi_1 - \arccos \frac{\cos(R_c/R) - \cos \theta_1 \cos \theta_0}{\sin \theta_1 \sin \theta_0} \\ \theta_{2u} &= \min\{\theta_{1u1}, \theta_{1u2}\} \\ \theta_{2u2} &= \arccos \left[\cos(R_c/R) / \sqrt{1 - \sin^2 \theta_0 \sin^2(\varphi_2 - \varphi_1)} \right] \\ & \quad + \arctan(\cos(\varphi_2 - \varphi_1) \tan \theta_1) \end{aligned}$$

Therefore, from (29), (30), (31) and (32), the lower bound shown in (3) can be derived.

As for the upper bound, replace $|S^-(\theta_0, \theta_1, \varphi_1)|$ by $|S^-(\theta_0, \theta_0, \varphi_1)|$, we can get the upper bound as illustrated in Section IV-B. ■

APPENDIX C
PROOF OF THEOREM 2

Comparing (3) to (12), (4) to (13), we can find that they are very similar. If we can show that each item related with R in (3) and (4) tends to its counterpart in (12) and (13) when $R \rightarrow \infty$, then it is easy to prove Theorem 2. For convenience, let $\theta_0 = r_0/R$, $\theta_1 = r_1/R$, $\varphi'_1 = \pi + \varphi_1$.

Proof: First, we have

$$\begin{aligned} & \lim_{R \rightarrow \infty} R \arccos([3 \cos^2(R_s/R) - 1]/2) \\ &= R_s \lim_{x \rightarrow 0} \frac{\arccos([3 \cos^2(x) - 1]/2)}{x} \quad (\text{let } x = R_s/R) \\ &\stackrel{(a)}{=} R_s \lim_{x \rightarrow 0} \frac{3 \cos x \sin x}{\sqrt{1 - ([3 \cos^2(x) - 1]/2)^2}} \\ &= R_s \lim_{x \rightarrow 0} \frac{6 \cos x \sin x}{\sqrt{(3 - 3 \cos^2 x)(1 + 3 \cos^2 x)}} = \sqrt{3} R_s \end{aligned} \quad (33)$$

where (a) follows from l'Hôpital's rule.

From (33), we know that when $R \rightarrow \infty$, the condition $R_c > R \arccos([3 \cos^2(R_s/R) - 1]/2)$ is equivalent to the condition $R_c > \sqrt{3} R_s$.

Similarly, we can get

$$\lim_{R \rightarrow \infty} R \theta_{0u} = \lim_{R \rightarrow \infty} R \arccos \sqrt{\frac{1 + 2 \cos(R_c/R)}{3}} = \frac{R_c}{\sqrt{3}} \quad (34)$$

Then, we can also obtain

$$\begin{aligned} & \lim_{R \rightarrow \infty} \arccos[(\cos(R_c/R) - \cos^2 \theta_0) / \sin^2 \theta_0] \\ &= \arccos\left(\lim_{R \rightarrow \infty} \frac{\cos(R_c/R) - \cos^2(r_0/R)}{\sin^2(r_0/R)}\right) \\ &\stackrel{(a)}{=} \arccos\left(\lim_{R \rightarrow \infty} \frac{\frac{R_c}{R^2} \sin \frac{R_c}{R} - \frac{2r_0}{R^2} \sin \frac{r_0}{R} \cos \frac{r_0}{R}}{-2r_0/R^2 \sin(r_0/R) \cos(r_0/R)}\right) \\ &= \arccos(1 - R_c^2/(2r_0^2)) \\ &\stackrel{(b)}{=} \pi - 2 \arccos(R_c/(2r_0)) \end{aligned} \quad (35)$$

where (a) uses l'Hôpital's rule and (b) follows from $\cos(\pi - 2 \arccos(R_c/(2r_0))) = 1 - R_c^2/(2r_0^2)$ and $0 \leq \pi - 2 \arccos(R_c/(2r_0)) \leq \pi$.

According to (35), comparing (5) to (14) and (15), we can get

$$\varphi_l(r_0) = \pi - \lim_{R \rightarrow \infty} \varphi_m(\theta_0) \quad (36)$$

$$\varphi_u(r_0) = \lim_{R \rightarrow \infty} 2\varphi_m(\theta_0) - \pi \quad (37)$$

Still using l'Hôpital's rule, we can get the following results. The detailed calculation is omitted due to space limitation.

$$\lim_{R \rightarrow \infty} R \theta_{1u1}(\theta_0, \varphi_1) = \sqrt{R_c^2 - r_0^2 \sin^2 \varphi'_1} - r_0 \cos \varphi'_1 \quad (38)$$

$$\begin{aligned} \lim_{R \rightarrow \infty} R \theta_{1u2}(\theta_0, \varphi_1) &= \sqrt{R_c^2 - r_0^2 \sin^2(\varphi'_1 + \varphi_l(r_0))} \\ &\quad + r_0 \cos(\varphi'_1 + \varphi_l(r_0)) \end{aligned} \quad (39)$$

where $\theta_{1u1}(\theta_0, \varphi_1)$ and $\theta_{1u2}(\theta_0, \varphi_1)$ are shown in (7) and (8).

From (38) and (39), comparing (6) to (16), we have

$$\lim_{R \rightarrow \infty} R \theta_{1u}(\theta_0, \varphi_1) = R_1(r_0, \varphi'_1) \quad (40)$$

From (36), (37) and (40), comparing (10) to (17) and by some simple replacement, we can obtain

$$\lim_{R \rightarrow \infty} |S^+(\theta_0, \varphi_1)| = |S^+(r_0, \varphi'_1)| \quad (41)$$

Similarly, we get

$$\lim_{R \rightarrow \infty} |S^-(\theta_0, \theta_1, \varphi_1)| = |S^-(r_0, r_1, \varphi'_1)| \quad (42)$$

where $|S^-(\theta_0, \theta_1, \varphi_1)|$ and $|S^-(r_0, r_1, \varphi'_1)|$ are shown in (11) and (18).

In addition, from (9), we have

$$\lim_{R \rightarrow \infty} |C(N, R\theta_0)| = \lim_{R \rightarrow \infty} 2\pi R^2(1 - \cos(r_0/R)) = \pi r_0^2 \quad (43)$$

Finally, using (34), (36), (37), (40), (41), (42) and (43), we can obtain from (3) that

$$\begin{aligned} \lim_{R \rightarrow \infty} p_l(\lambda) &= \lim_{R \rightarrow \infty} 2\pi \lambda^2 \int_{R_s}^{R\theta_{0u}} R \sin \frac{r_0}{R} dr_0 \int_{\pi - \varphi_m(\theta_0)}^{2\varphi_m(\theta_0) - \pi} d\varphi'_1 \\ &\quad \int_{R\theta_0}^{R\theta_{1u}(\theta_0, \varphi_1)} R \sin \frac{r_1}{R} \times e^{-\lambda \pi r_0^2} e^{-\lambda |S^+(r_0, \varphi'_1)|} \\ &\quad \times (1 - e^{-\lambda |S^-(r_0, r_1, \varphi'_1)|}) dr_1 \\ &= 2\pi \lambda^2 \int_{R_s}^{R_c/\sqrt{3}} r_0 dr_0 \int_{\varphi_l(r_0)}^{\varphi_u(r_0)} d\varphi'_1 \int_{r_0}^{R_1(r_0, \varphi'_1)} e^{-\lambda \pi r_0^2} \\ &\quad \times e^{-\lambda |S^+(r_0, \varphi'_1)|} (1 - e^{-\lambda |S^-(r_0, r_1, \varphi'_1)|}) r_1 dr_1 \\ &= p'_l(\lambda) \end{aligned}$$

Similarly, we can get $\lim_{R \rightarrow \infty} p_u(\lambda) = p'_u(\lambda)$. ■

REFERENCES

- [1] G. Werner-Allen, K. Lorincz, M. Welsh, O. Marcillo, J. Johnson, M. Ruiz, and J. Lees, "Deploying a wireless sensor network on an active volcano," *IEEE Internet Computing*, vol. 10, no. 2, pp. 18–25, March 2006.
- [2] L. Mo, Y. He, Y. Liu, J. Zhao, S.-J. Tang, X.-Y. Li, and G. Dai, "Canopy closure estimates with greenorbs: sustainable sensing in the forest," in *Proc. ACM SenSys*, Berkeley, CA, USA, Nov. 2009, pp. 99–112.
- [3] P. Gupta and P. R. Kumar, "The capacity of wireless networks," *IEEE Trans. Inf. Theory*, vol. 46, no. 2, pp. 388–404, Mar. 2000.
- [4] Q. Fang, J. Gao, and L. Guibas, "Locating and bypassing routing holes in sensor networks," in *Proc. IEEE INFOCOM*, vol. 4, Hong Kong, China, Mar. 2004, pp. 2458–2468.
- [5] G. Wang, G. Cao, and T. La Porta, "Movement-assisted sensor deployment," in *Proc. IEEE INFOCOM*, vol. 4, Hong Kong, China, Mar. 2004, pp. 2469–2479.
- [6] C. Zhang, Y. Zhang, and Y. Fang, "Localized algorithms for coverage boundary detection in wireless sensor networks," *Wirel. Netw.*, vol. 15, no. 1, pp. 3–20, Jan. 2009.
- [7] C. Huang and Y. Tseng, "The coverage problem in a wireless sensor network," in *Proc. ACM WSNA*, San Diego, California, USA, Sep. 2003, pp. 115–121.
- [8] C.-F. Huang, Y.-C. Tseng, and L.-C. Lo, "The coverage problem in three-dimensional wireless sensor networks," in *Proc. IEEE Globecom*, vol. 5, Dallas, Texas, Dec. 2004, pp. 3182–3186.
- [9] Y. Bejerano, "Simple and efficient k-coverage verification without location information," in *Proc. IEEE INFOCOM*, Phoenix, Arizona, USA, Apr. 2008, pp. 897–905.
- [10] —, "Coverage verification without location information," *IEEE Trans. Mobile Comput.*, vol. 11, no. 4, pp. 631–643, Apr. 2012.
- [11] V. de Silva, R. Ghrist, and A. Muhammad, "Blind swarms for coverage in 2-d," in *Proc. Robotics: Science and Systems*, Cambridge, MA, Jun. 2005, pp. 335–342.
- [12] V. de Silva and R. Ghrist, "Coverage in sensor networks via persistent homology," *Algebraic & Geometric Topology*, vol. 7, pp. 339–358, 2007.

- [13] R. Ghrist and A. Muhammad, "Coverage and hole-detection in sensor networks via homology," in *Proc. 4th International Conference on Information Processing in Sensor Networks*, Los Angeles, California, USA, Apr. 2005, pp. 254–260.
- [14] F. Chazal and S. Y. Oudot, "Towards persistence-based reconstruction in euclidean spaces," in *Proc. ACM SCG*, ser. SCG '08. College Park, MD, USA: ACM, Jun. 2008, pp. 232–241.
- [15] A. Muhammad and M. Egerstedt, "Control using higher order laplacians in network topologies," in *Proc. 17th International Symposium on Mathematical Theory of Networks and Systems*, Kyoto, Japan, Jul. 2006, pp. 1024–1038.
- [16] A. Muhammad and A. Jadbabaie, "Decentralized computation of homology groups in networks by gossip," in *Proc. American Control Conference*, New York, NY, USA, Jul. 2007, pp. 3438–3443.
- [17] A. Tahbaz-Salehi and A. Jadbabaie, "Distributed coverage verification in sensor networks without location information," *IEEE Trans. Autom. Control*, vol. 55, no. 8, pp. 1837–1849, Aug. 2010.
- [18] B. Liu and D. Towsley, "A study of the coverage of large-scale sensor networks," in *Proc. IEEE MASS*, Fort Lauderdale, Florida, USA, Oct. 2004, pp. 475–483.
- [19] P.-J. Wan and C.-W. Yi, "Coverage by randomly deployed wireless sensor networks," *IEEE Trans. Inf. Theory*, vol. 52, no. 6, pp. 2658–2669, Jun. 2006.
- [20] D. Moltchanov, "Distance distributions in random networks," *Ad Hoc Netw.*, vol. 10, no. 6, pp. 1146–1166, Aug. 2012.
- [21] L. Lazos and R. Poovendran, "Stochastic coverage in heterogeneous sensor networks," *ACM Trans. Sen. Netw.*, vol. 2, no. 3, pp. 325–358, Aug. 2006.
- [22] M.-C. Zhao, J. Lei, M.-Y. Wu, Y. Liu, and W. Shu, "Surface coverage in wireless sensor networks," in *Proc. IEEE INFOCOM*, Rio de Janeiro, Brazil, Apr. 2009, pp. 109–117.
- [23] L. Liu and H. Ma, "On coverage of wireless sensor networks for rolling terrains," *IEEE Trans. Parallel Distrib. Syst.*, vol. 23, no. 1, pp. 118–125, Jan. 2012.
- [24] X. Li, D. K. Hunter, and S. Zuyev, "Coverage properties of the target area in wireless sensor networks," *IEEE Trans. Inf. Theory*, vol. 58, no. 1, pp. 430–437, Jan. 2012.
- [25] F. Yan, P. Martins, and L. Decreusefond, "Accuracy of homology based approaches for coverage hole detection in wireless sensor networks," in *Proc. IEEE ICC*, Ottawa, Canada, Jun. 2012, pp. 497–502.
- [26] M. A. Armstrong, *Basic Topology*. Springer, 1983.
- [27] J. Munkres, *Elements of algebraic topology*. Addison-Wesley, 1984.
- [28] A. Hatcher, *Algebraic Topology*. Cambridge University Press, 2002.
- [29] R. Bott and L. W. Tu, *Differential Forms in Algebraic Topology*. Springer-Verlag, 1982.



Philippe Martins received a M.S. degree in signal processing and another M.S. degree in networking and computer science from Orsay University and ESIGETEL France, in 1996. He received the Ph.D. degree with honors in electrical engineering from Telecom ParisTech, Paris, France, in 2000.

He is currently a Professor in the Network and Computer Science Department, at Telecom ParisTech. His main research interests lie in performance evaluation in wireless networks (RRM, scheduling, handover algorithms, radio metrology). His current investigations address mainly three issues: a) the design of distributed sensing algorithms for cognitive radio b) distributed coverage holes detection in wireless sensor networks c) the definition of analytical models for the planning and the dimensioning of cellular systems. He has published several papers on different international journals and conferences. He is also an IEEE senior member and he is co-author of several books on 3G and 4G systems.



Laurent Decreusefond is a former student of Ecole Normale Supérieure de Cachan. He obtained his Ph.D. degree in Mathematics in 1994 from Telecom ParisTech and his Habilitation in 2001. He is currently a Professor in the Network and Computer Science Department, at Telecom ParisTech. His main fields of interest are the Malliavin calculus, the stochastic analysis of long range dependent processes, random geometry and topology and their applications. With P. Moyal, he co-authored a book about the stochastic modelling of telecommunication

systems.



Feng Yan received the B.S. degree from Huazhong University of Science and Technology, China, in 2005 and the M.S. degree from Southeast University, China, in 2008, both in electrical engineering. He received the Ph.D. degree in 2013 from Telecom ParisTech, Paris, France. He is currently a postdoc in Telecom Bretagne, Rennes, France. His current research interests are in the areas of wireless communications and wireless networks, with emphasis on applications of homology theory, stochastic geometry in wireless networks.